Tunneling ionization of the ^{4}F and ^{6}D states of vanadium: Exchange blockade

Xi Chu and Gerrit C. Groenenboom

Tunneling ionization of the ^4F and ^6D states of vanadium: exchange blockade

Xi Chu

Department of Chemistry and Biochemistry,

The University of Montana, Missoula, Montana 59812

Gerrit C. Groenenboom

Institute for Molecules and Materials,

Radboud University Nijmegen, Heyendaalseweg 135,

6525 AJ Nijmegen, The Netherlands

(Dated: June 28, 2017)

Abstract

Using TDDFT calculations we compare tunneling ionization of the a^4F ground state and the a^6D first excited state of vanadium in laser fields of intensities between 1.4 and $4.0{\times}10^{13}$ W/cm^2. The calculated ionization yields of the ground state of vanadium were already shown to agree well with experimental results [Chu and Groenenboom, Phys. Rev. A **94**, 053417 (2016)]. We find that the tunneling ionization rate of the sextet state is lower than that of the quartet state. This is surprising, since the ionization potential of the sextet is lower than that of the quartet state. This finding, however, is consistent with the experimental observation that niobium, whose ground state is $a^6D_{1/2}$, has a much smaller ionization yield than vanadium ($a^4F_{3/2}$), even though their ionization potentials are extremely close [Smits *et al.*, Phys. Rev. Lett. **93**, 213003 (2004)]. Our calculations demonstrate the existence of exchange blockade for the higher spin state. It arises from a strong field dynamic effect that the highest and second highest electrons mixing in the same set of unoccupied spin orbitals, which causes an isotropic attractive potential that confines the electrons close to the core.

I. INTRODUCTION

The emerging field of attosecond science [1, 2] is based on the interaction of atoms and molecules with intense lasers. Currently, strong field theories often use the single active electron (SAE) approximation. Among these theories are the widely adopted strong field approximation [3] and the Ammosov-Delone-Kralnov (ADK) tunneling ionization [4] model. While SAE based approaches have been successful in describing the interaction of inert gases with strong fields, more and more work on molecules reveals the involvement of orbitals lower in energy than the highest occupied orbital [5, 6], suggesting the importance of many-electron mechanisms. Such involvement is usually related to the polarization direction of laser field in the molecular frame [7]. Sometimes resonances in photoelectron spectra also show up in high harmonic generation [6, 8], indicating similar many-electron mechanisms.

Atoms and molecules ionize through tunneling in intense laser fields. Tunneling ionization yields for transition metal atoms V, Ni, Pd, Ta, and Nb are significantly lower than the ADK predictions [9, 10]. In particular V and Nb belong to the same group in the periodic table and their ionization potentials differ by only 0.01 eV. And yet, the measured saturation intensity of Nb is twice as large as that for V [10]. Even though the polarizability of Nb is larger by 27%, tunneling models that take polarizability into consideration cannot explain the particularly large ionization suppression in Nb compared to V [11–13].

A notable difference between the electronic structure of V and Nb is that the ground state of V is $(3d^34s^2)^4F$ and that of Nb is $(4d^45s)^6D$. To our best knowledge, there has not been any publications addressing the relationship between the spin state and tunneling ionization. In order to determine whether a higher spin multiplicity could be the cause of reduced ionization, we employ a method that takes electron spin into consideration.

In an earlier study, we applied a time-dependent density functional theory (TDDFT) method to calculate the ionization yields of vanadium in intense laser fields [14]. Results of our calculation agreed well with measurements in the tunneling regime of single ionization. Our work confirmed the proposal that the multielectron response exerts an additional barrier for tunneling [10]. Specifically, we found that the isotropic component and the dipole component of the induced potential contribute the most to reducing the tunneling rate. As the electron density moves away from the nucleus in a laser field, an isotropic attractive potential is created at the core, which effectively reduces the energy of the electron in the

highest occupied orbital and hence increases the ionization potential. Meanwhile, momentary accumulation and depletion of the electron density of one side of the nucleus versus the other gives rise to the dipole component that elevates the barrier at medium to large radial distances.

With a similar method we here study the role of spin multiplicity in tunneling ionization. Rather than comparing the ^4F state of vanadium with the ^6D state of niobium, we study the ^4F and ^6D states of vanadium that can be represented with a single Slater determinant. The advantage of this scheme is that it avoids errors associated with adding a complete atomic shell. In our model the ionization potential of the ^4F quartet state is slightly higher than that of the ^6D sextet state. Were ionization potential the only determining factor, tunneling ionization rates of the sextet would be higher. However, both the experimental results and our earlier study point to the importance of many-electron responses. This work, therefore, amounts to a comparison of the many electron responses of states with different spin multiplicities.

Vanadium exists in many oxidation states V^{2+}, V^{3+}, V^{4+}, V^{5+} so it functions as an electron transfer catalyst in a wide variety of reactions. In computational chemistry, modeling these metallic compounds largely relies on DFT, usually employing a hybrid exchange-correlation potential that reproduces bond distances and energies well. For time-dependent calculations of atomic ionization, it is important that the negative of the orbital energy is consistent with the ionization energy. Also, the long range singularity and the anisotropy of the open-shell atom must correctly be accounted for to calculate tunneling ionization.

Our earlier TDDFT work suggested that only when the field is relatively weak and the Keldysh parameter is greater than 1.1, correlation effects are important in determining ionization rates and outcome [14]. Ionization is multiphoton, rather than tunneling, in this regime. Our inclusion of the correlation potential was not sufficient to describe the effect that arises from multiple electron configurations in this case. However, when the laser intensity is greater and ionization is dominated by tunneling, TDDFT calculations reproduced the measured ionization yields for a range of laser intensity. Analysis of the data showed that the included correlation potential played little role in the many-body effects that reduce the tunneling ionization. In the present comparative study we drop the correlation term and approximate the time-dependent exchange-correlation potential as a weighted average of Hartree Fock exchange potentials between occupied orbitals. Designed as such, this work

specifically investigates the relationship between the spin state of transition metal atoms and the Coulomb and exchange potentials in intense laser fields. Its conclusions may be applicable to a class of open shell atoms and molecules.

In the following section we introduce a SAE model that is based on the static Kohn-Sham (KS) equations. In Section III we briefly describe our all electron TDDFT method and the multipole expansion of the KS potentials, which we use in analysis of the results. In Section IV we present the results of the static DFT calculations, the ionization rates computed with a SAE model, and the results for the all electron TDDFT calculation. In Section V we analyse the TDDFT results and identify the mechanism that explains the suppression of tunneling ionization in the high spin state. Finally, in Section VI we briefly discuss spin contamination and we conclude.

II. SINGLE ACTIVE ELECTRON APPROXIMATION BASED ON DFT

The states of the neutral atoms before ionization are obtained from static DFT calculations. To solve the static KS equations, we use the generalized pseudospectral method [15] that puts more grid points near the nucleus and fewer near the cutoff, which is at 1000 a_0. In the ionization calculations an absorbing boundary, which models the ionization process, is placed at 75 a_0. Calculations are converged with respect to all adjustable parameters. We use a spin-unrestricted formalism, so the orbital energies for spin up ($\uparrow$) and spin down ($\downarrow$) electrons can be different. The difference mostly arises from the exchange-correlation potential, since the Coulomb potential is spin independent. Our convention is to have more electrons in the α spin states, i.e. $N_\uparrow > N_\downarrow$. Further details of the method are given in reference [14].

Assuming that intense laser fields do not alter the ion-electron interaction, i.e., there is not any laser induced potential for the active electron, we approximate the time-dependent KS potential as

$$v_\sigma(\boldsymbol{r}, t) = v_\sigma(\boldsymbol{r}, 0) + \mathbf{E}(t) \cdot \boldsymbol{r}, \tag{1}$$

where σ is the spin index and $\boldsymbol{r}$ is the electron coordinate. The polarization direction of the electric field $\mathbf{E}$ is along the z axis and

$$E(t) = f(t) \sin \omega t, \tag{2}$$

4

where ω is the angular frequency of the incident light and $f(t)$ is the field strength for which we use $\sin^2$ pulses of 20 optical cycles. For 1500 nm lasers, the pulse duration is 100 fs.

To obtain the ionization yields, we solve the time-dependent equations

$$i\frac{\partial}{\partial t}\psi_{i\sigma}(\boldsymbol{r},t) = \left[\hat{H}_\sigma^0(\boldsymbol{r}) + \boldsymbol{E}(t)\cdot\boldsymbol{r}\right]\psi_{i\sigma}(\boldsymbol{r},t),$$
$$i = 1, 2, \ldots, N_\sigma, \tag{3}$$

where i is the orbital index, N_σ is the number of electrons for the σ spin, and $\psi_{i\sigma}$ is the time-dependent spin orbital. Initially $\psi_{i\sigma}(\boldsymbol{r},0)$ is a solution of the static KS equations whose Hamiltonian is $\hat{H}_\sigma^0(\boldsymbol{r})$.

All the occupied spin orbitals are propagated in time. We calculate the survival probability for each spin orbital as

$$n_{i\sigma} = \iiint \psi_{i\sigma}^*(\boldsymbol{r},T)\psi_{i\sigma}(\boldsymbol{r},T)d^3\mathbf{r}, \tag{4}$$

where T is the pulse length and the ionization probability for each spin orbital as

$$\gamma_{i\sigma} = 1 - n_{i\sigma}. \tag{5}$$

The ionization yield is calculated as the sum

$$P = \sum_\sigma \sum_{i=1}^{N_\sigma} \gamma_{i\sigma}. \tag{6}$$

III. TDDFT MODELING OF THE STRONG FIELD INDUCED POTENTIAL

Zangwill and Soven have shown that in the linear response regime, the potential change due to many electron effects must be included to properly reproduce the polarizability and photoabsorption cross section of rare gas atoms [16]. Similarly, in our previous work on the $^4F_{9/2}$ state of vanadium [14] we have shown that in intense laser fields, instead of Eq. (1), we should use the time-dependent KS potential

$$v_\sigma(\boldsymbol{r},t) = v_\sigma(\boldsymbol{r},0) + \Delta v_\sigma(\boldsymbol{r},t) + \boldsymbol{E}(t)\cdot\boldsymbol{r}, \tag{7}$$

in which $\Delta v_\sigma(\boldsymbol{r},t)$ is the induced potential. Depending on the laser intensity, the impact of $\Delta v_\sigma(\boldsymbol{r},t)$ may be as large as effectively increasing the ionization potential by 1 eV.

In our TDDFT method we describe the induced KS potentials $\Delta v_\sigma(\boldsymbol{r},t)$ by

$$\Delta v_\sigma(\boldsymbol{r},t) = \iiint \frac{\Delta\rho(\boldsymbol{r}',t)}{|\boldsymbol{r}-\boldsymbol{r}'|}d^3\boldsymbol{r}' + \Delta V_{\mathrm{xc},\sigma}(\boldsymbol{r},t), \tag{8}$$

where $\Delta\rho$ and $\Delta V_{\mathrm{xc},\sigma}$ are the changes in the electron density and exchange-correlation potential relative to their respective initial values. Evaluating them involves solving time-dependent KS equations

$$i\frac{\partial}{\partial t}\psi_{i\sigma}(\boldsymbol{r},t) = \left[\hat{H}_\sigma^0(\boldsymbol{r}) + \Delta v_\sigma(\boldsymbol{r},t) + \boldsymbol{E}(t)\cdot\boldsymbol{r}\right]\psi_{i\sigma}(\boldsymbol{r},t),$$
$$i = 1, 2, \ldots, N_\sigma. \tag{9}$$

The electron spin density at coordinate $\boldsymbol{r}$ and time t is determined by the set of occupied orbitals $\{\psi_{i\sigma}\}$ as

$$\rho_\sigma(\boldsymbol{r},t) = \sum_{i=1}^{N_\sigma}\psi_{i\sigma}^*(\boldsymbol{r},t)\psi_{i\sigma}(\boldsymbol{r},t). \tag{10}$$

The change in electron density is

$$\Delta\rho(\boldsymbol{r},t) = \sum_{\sigma=\alpha}^{\beta}\rho_\sigma(\boldsymbol{r},t) - \rho_\sigma(\boldsymbol{r},0), \tag{11}$$

in which $\rho_\sigma(\boldsymbol{r},0)$ is calculated from the initial spin orbitals that are solutions of the static KS equations.

The time-dependent exchange-correlation potential is expressed as

$$V_{\mathrm{xc},\sigma}(\boldsymbol{r},t) = -\frac{1}{\rho_\sigma(\mathbf{r},t)}\sum_i\sum_j\mathrm{Re}\left[\psi_{j\sigma}^*(\boldsymbol{r},t)\psi_{i\sigma}(\boldsymbol{r},t)\iiint\frac{\psi_{i\sigma}^*(\boldsymbol{r}',t)\psi_{j\sigma}(\boldsymbol{r}',t)}{|\mathbf{r}-\mathbf{r}'|}d^3\boldsymbol{r}'\right]. \tag{12}$$

The change in the exchange-correlation potential, ΔV_{xc}, is

$$\Delta V_{\mathrm{xc},\sigma}(\boldsymbol{r},t) = V_{\mathrm{xc},\sigma}(\boldsymbol{r},t) - V_{\mathrm{xc},\sigma}(\boldsymbol{r}), \tag{13}$$

where $V_{\mathrm{xc},\sigma}(\boldsymbol{r})$ is the exchange-correlation potential in the static KS equation. Its expression is given in reference [14].

The time-dependent KS equations in Eq. (9) are Euler equations resulting from the quantum action [17, 18]

$$A[\Psi] = \int_{t_0}^{t_1}dt\left\langle\Psi(t)|i\frac{\partial}{\partial t} - \hat{H}(t)|\Psi(t)\right\rangle \tag{14}$$

having a stationary point at the time-dependent density $\rho(\boldsymbol{r},t)$. In Eq. (14), $\Psi(t)$ is the total N-electron wave function and it is represented by the Slater determinant,

$$\Psi(t) = \frac{1}{\sqrt{N!}}\det\left[\psi_{1\sigma_1}(t)\psi_{2\sigma_2}(t)\cdots\psi_{N\sigma}(t)\right]. \tag{15}$$

6

Projecting Eq. (15) onto a determinant of field free orbitals, we find contributions of single, double, triple, and higher excitations. Such multiple excitations/de-excitations are many-electron by nature and they cause $\Delta\rho$ and ΔV_{xc} in Eq. (8).

To solve Eqs. (9) we employ the time-dependent generalized pseudospectral method [14, 19].

A. Legendre expansion of the induced Kohn-Sham potentials

In the analysis of the TDDFT results below we will employ a Legendre expansion of the induced KS potentials $\Delta v_\sigma(\boldsymbol{r}, t)$, since in previous work we found that only the lowest two orders have an appreciable effect in the time-dependent equations [14].

The expansion is

$$\Delta v_\sigma(\boldsymbol{r}, t) = \sum_{l=0}^{\infty} \Delta v_\sigma^{(l)}(r, t) P_l(\cos\theta), \tag{16}$$

where P_l is a Legendre polynomial of order l, θ is the angle between the vector $\boldsymbol{r}$ and laser polarization $\boldsymbol{E}$, and the expansion coefficients $\Delta v_\sigma^{(l)}(r, t)$ depend on the distance $r = |\boldsymbol{r}|$. To find the expansion coefficients we use the multipole expansion of the Coulomb interaction:

$$\frac{1}{|\boldsymbol{r} - \boldsymbol{r}'|} = \sum_{l=0}^{\infty} \sum_{m=-l}^{l} \frac{4\pi}{2l+1} \frac{r_<^l}{r_>^{l+1}} Y_{lm}(\hat{r})^* Y_{lm}(\hat{r}'), \tag{17}$$

where $r_<$ is the smaller of r and r' and $r_>$ is the larger of the two, Y_{lm} are spherical harmonics, and $\hat{r}$ and $\hat{r}'$ are the spherical polar coordinates of $\boldsymbol{r}$ and $\boldsymbol{r}'$, respectively. Substituting this expansion into Eq. (12), using the orthogonality relations for spherical harmonics and Legendre polynomials gives for the Coulomb term

$$\Delta v_\beta(\boldsymbol{r}, t) \approx \frac{\int_0^r \Delta\rho_\alpha^{(0)}(r', t) dr'}{r} + \int_r^\infty \frac{\Delta\rho_\alpha^{(0)}(r', t)}{r'} dr' + \left[\frac{\int_0^r \Delta\rho_\alpha^{(1)}(r', t) r' dr'}{r^2} + r \int_r^\infty \frac{\Delta\rho_\alpha^{(1)}(r', t)}{r'^2} dr' \right] \cos(\theta), \tag{18}$$

where $\Delta\rho_\alpha^{(l)}(r, t)$ are the coefficients in the Legendre expansion of $\Delta\rho_\alpha(\boldsymbol{r}, t)$.

The exchange term can be expanded in a similar way by introducing a Legendre expansion for the orbital products in Eq. (12)

$$\rho_{i\sigma, j\sigma}(\boldsymbol{r}, t) = \psi_{i\sigma}(\boldsymbol{r}, t) \psi_{j\sigma}^*(\boldsymbol{r}, t) = \sum_{l=0}^{\infty} \rho_{i\sigma, j\sigma}^{(l)}(r, t) P_l(\cos\theta). \tag{19}$$

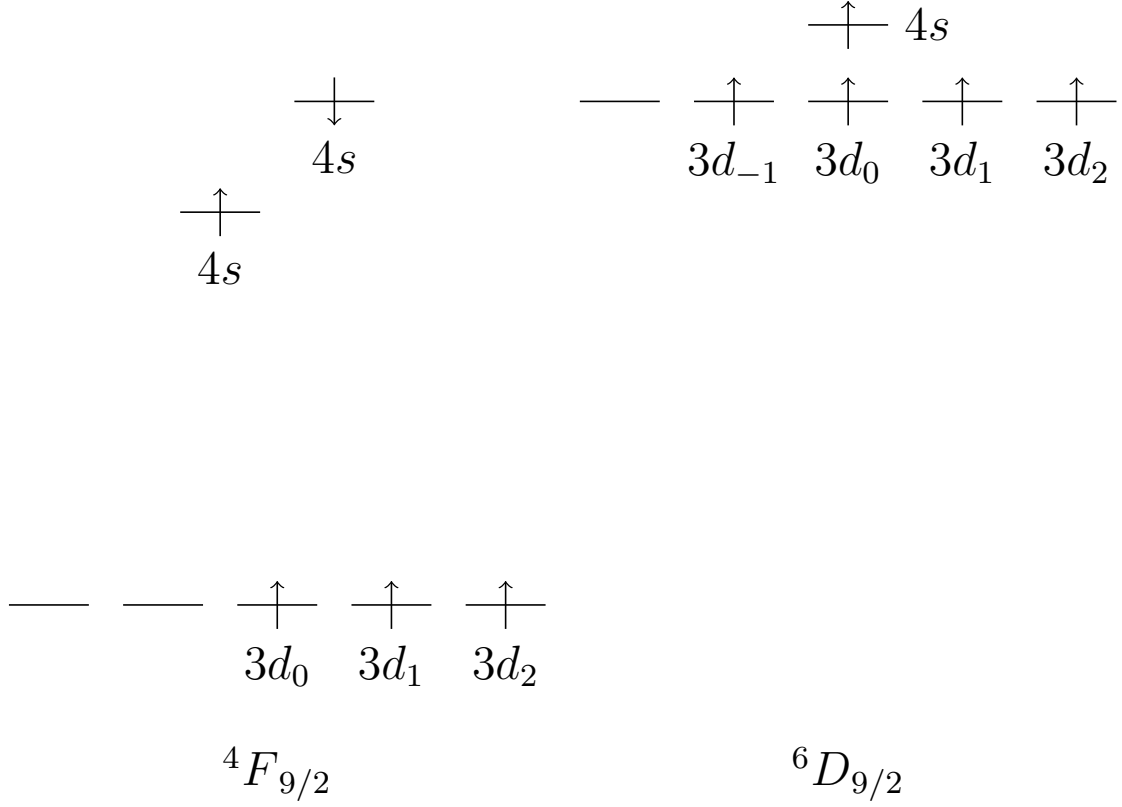We give the explicit expressions in Section V below.

Figure 1: Orbital energy level diagrams for the vanadium $(3d^3 4s^2)^4F_{9/2}$ and $(3d^4 4s)^6D_{9/2}$ states.

Table I: Calculated orbital energies (ϵ) in eV of vanadium compared to measured ionization potential (I_p) from Ref. [20].

Neutral		Cation				
State	Conf.	State	Conf.	I_p	Orbital	$-\epsilon$
$^4F_{\frac{9}{2}}$	$3d^3 4s^2$	$^5F_5$	$3d^3 4s$	7.07	$4s_\downarrow$	6.99
		$^3F_4$	$3d^3 4s$	7.81	$4s_\uparrow$	7.96
		$^3F_4$	$3d^2 4s^2$	11.5	$3d_\uparrow$	11.4
$^6D_{\frac{9}{2}}$	$3d^4 4s$	$^5D_4$	$3d^4$	6.49	$4s_\uparrow$	6.52
		$^5F_5$	$3d^3 4s$	6.84	$3d_\uparrow$	6.99

IV. RESULTS

A. Static DFT calculations

We study the $(3d^3 4s^2)^4F$ and $(3d^4 4s)^6D$ terms of vanadium (Fig. 1). The ground state is $^4F_{3/2}$, but we focus on the $^4F_{9/2}$ and $^6D_{9/2}$ fine structure levels, which are $0.068\,558$ and $0.30\,0634$ eV above the ground state [20], respectively. These states can be presented by a single Slater determinant, which allows us to use TDDFT calculations to compare the tunneling ionization processes of quartet and sextet states.

In Table I we list the calculated orbital energies, together with the measured ionization potentials for removing an electron from those orbitals while keeping other electrons in the same spin orbitals as in the neutral atoms. The ionization of the quartet changes the ground state electronic configuration into an excited state configuration of the cation. For the sextet it is the other way around: the cation is in its ground state configuration, while the neutral is in an excited state. As a result, the single electron ionization potential of the quartet is higher than that of the sextet by 0.5 eV. The calculate and measured ionization energies agree well.

B. Ionization in the DFT based single active electron approximation

Figure 2 shows a comparison of the ionization yields of the $^6D_{9/2}$ and $^4F_{9/2}$ states under the assumption that the potential from the ion does not change with time. As expected in this approximation, the sextet state has a higher ionization yield due to its lower ionization potential.

Only the highest occupied spin orbitals contribute significantly to the ionization yield calculated with Eq. (6). For the $^4F_{9/2}$ quartet it is $4s_\downarrow$. For the $^6D_{9/2}$ sextet $4s_\uparrow$ is the highest. Figure 3 shows these orbitals, together with their corresponding KS potentials. The potentials include the attractive interaction with the nucleus, the Coulomb repulsion term from the total electron density, and the exchange-correlation term. The KS potential of the sextet is higher for $r < 2.30\ a_0$ while the potentials become very similar for $r \geq 5.09\ a_0$. The higher energy of the sextet results in a higher ionization rate when the intense laser field is switched on and the electron-ion potential is kept constant.
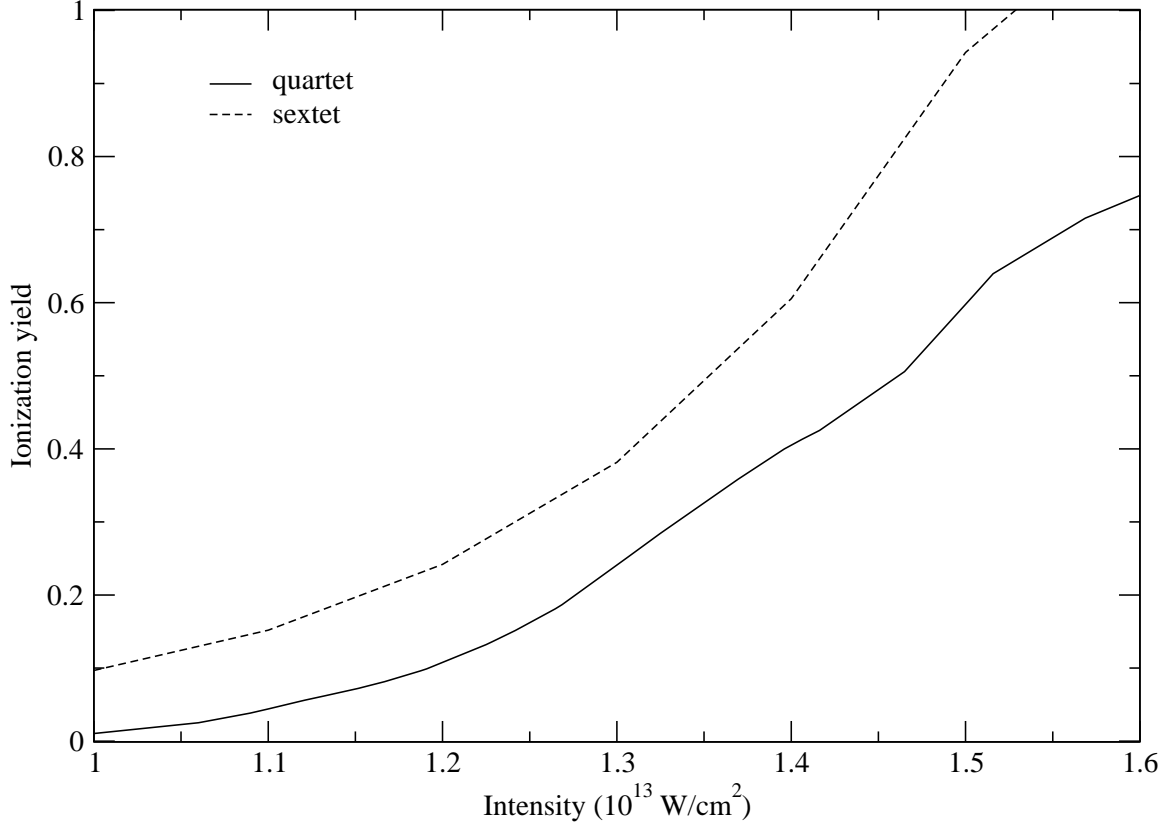
Figure 2: Calculated ionization yield of the ${}^4F_{9/2}$ quartet and ${}^6D_{9/2}$ sextet states of vanadium in 1500 nm 100 fs laser pulses, when induced potentials are not included [see Eq. (3)].

C.   TDDFT prediction of ionization yields

In Fig. 4 we plot the calculated ionization yields for the ${}^4F_{9/2}$ quartet and ${}^6D_{9/2}$ sextet by the all electron TDDFT method. From 1.4 to 2.5×10^{13} W/cm^2 intensity, the values for the quartet was shown to agree with measurements [14]. Here, we only present yields that are less than 0.5, which, from TDDFT calculations, should be more reliable than higher yields. In contrast with the comparison in Fig. 2, the ionization yields are much lower for the sextet than for the quartet. Inclusion of many-electron dynamics reduces the ionization yield for both the quartet and sextet, but the reduction for sextet is much greater.

In the next section we analyse the many-electron dynamics and show that the exchange interaction between time propagated $4s_\uparrow$ and $3d_\uparrow$ electrons strongly affects tunneling ionization of the sextet. It creates a temporal attractive potential that is spatially isotropic and narrow, which binds the electron closer to the core and effectively increases the ionization potential.
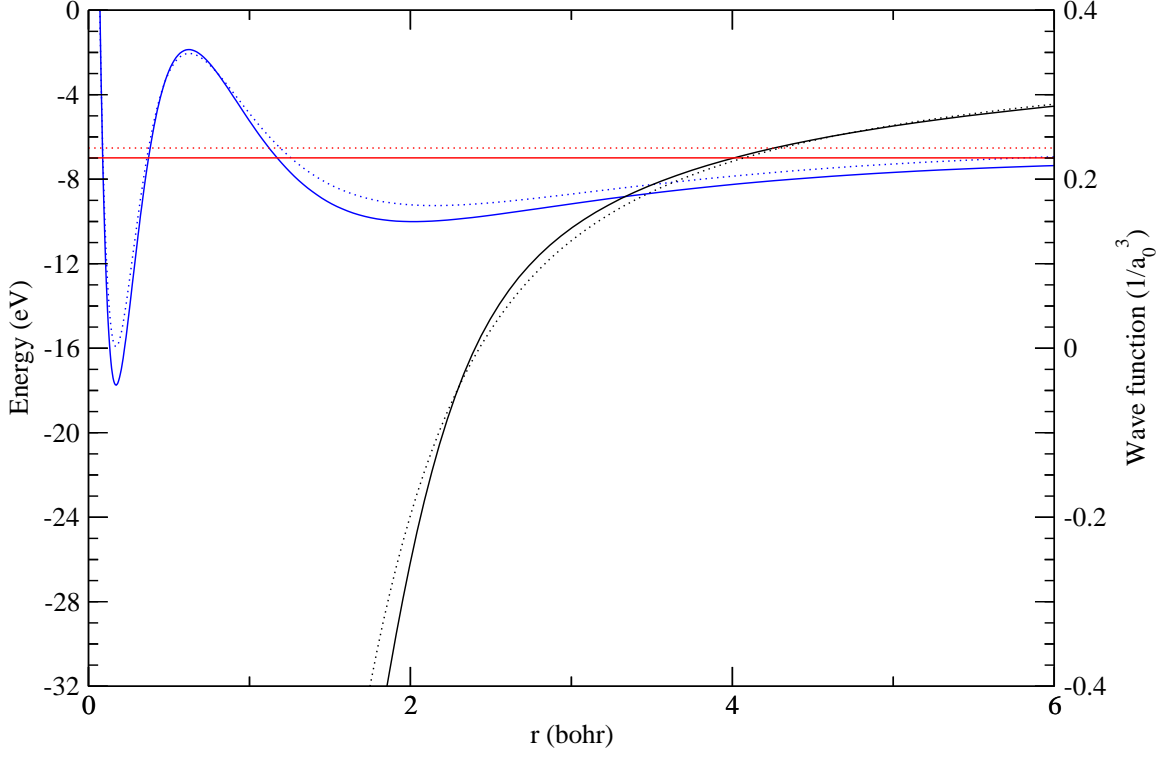
Figure 3: Comparison of the Kohn-Sham potentials (black), the highest spin orbital (blue) and its energy (red) of the $^4F_{9/2}$ and $^6D_{9/2}$ states. The solid lines refer to $^4F_{9/2}$ and the dotted lines to $^6D_{9/2}$. The wave functions are shifted vertically such that their zeros occur at the intersections with the corresponding energy levels.

V.   ANALYSIS OF TDDFT MANY-ELECTRON DYNAMICS

Equation (8) shows that the changes in the spin-dependent KS potentials Δv_σ are related to the change in the electron density $\Delta\rho$ and the changes in the spin-dependent exchange-correlation potentials $\Delta V_{\mathrm{xc},\sigma}$ as induced by the intense laser field. Even if only one electron is active, these two terms are nonzero. But at least at large radial distances, where the active electron dominates the density, the two terms cancel. This can be seen from Eq. (12) by letting i and j correspond to the highest occupied spin orbital, which give minus the Coulomb integral. At small radial distances many electrons contribute to the density, so the change due to the active electron is small.

Hence when comparing the predictions of the SAE model [Eq. (3)] and the TDDFT approach [Eq. (9)], we deduce that many-electron dynamics gives rise to a Δv_σ contribution, which results in substantial suppression of the ionization. In the TDDFT calculations all
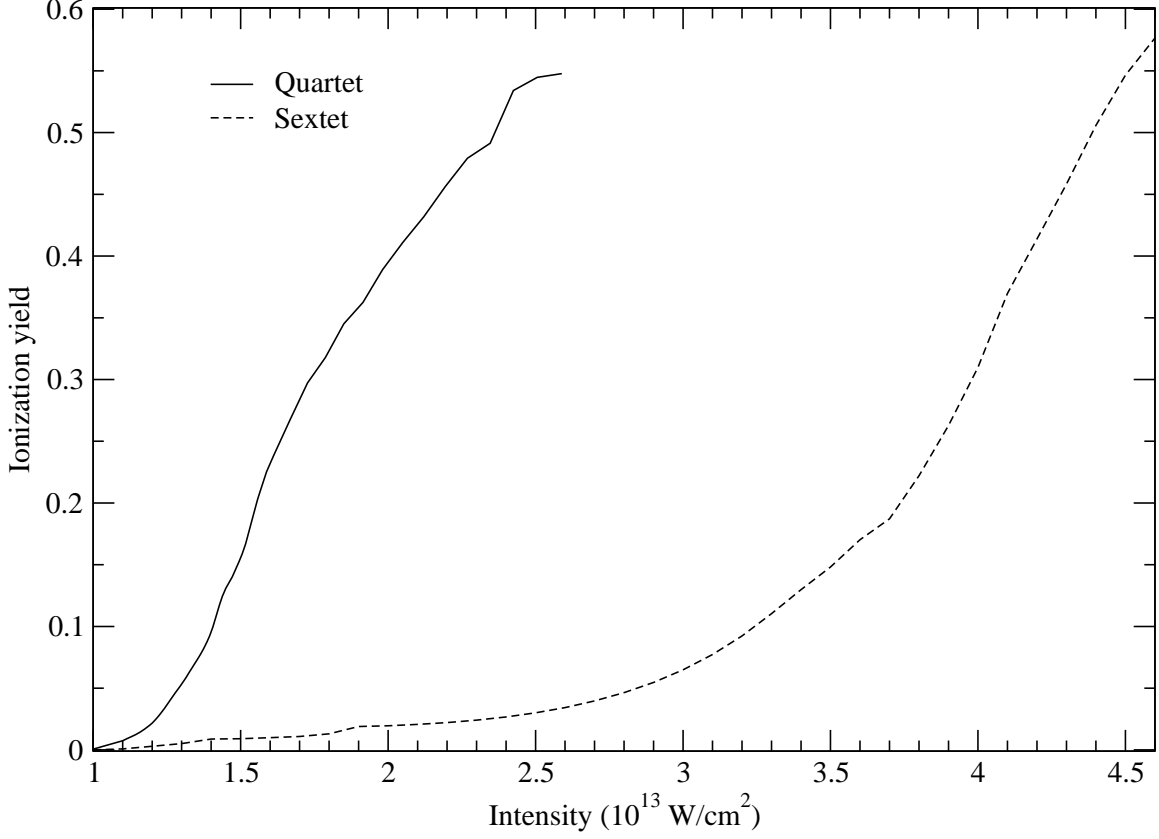
11

Figure 4: The ionization yield of the $^4F_{9/2}$ and $^6D_{9/2}$ states of vanadium in 1500 nm lasers as a function of the laser intensity, calculated with the all electron TDDFT method [see Eq. (9)].

electrons were included, but in this analysis we focus on the Δv_σ contributions that are caused by the dynamics of electrons that occupy the second highest spin orbitals. For the $^4F_{9/2}$ quartet state this is the $4s_\uparrow$ orbital, and for the sextet state these are the $3d_\uparrow$ orbitals. For the quartet state, the $4s_\downarrow$ electron that ionizes has β spin, so its dynamics is controlled by the v_β potential, which only depends on the $4s_\uparrow$ electron through the Coulomb term. Whereas for the $^6D_{9/2}$ sextet state, exchange interaction contributes since the $4s_\uparrow$ ionizing electron has the same spin as the $3d_\uparrow$ electrons.

For the quartet state, the electron which is initially in the $4s_\uparrow$ orbital is subject to the more attractive potential v_α (see Fig. 5). Nonetheless, it moves away from the core in an intense laser field, which makes $\Delta\rho_\alpha^{(0)}$ negative for small radial distances. Hence, the sum of the first two terms in Eq. (18) is negative, which means that $\Delta v_\beta^{(0)}$ is attractive, particularly near the core. Following the electric field of the laser, $\Delta\rho_\alpha^{(1)}$ peaks at a somewhat larger radial distance, which creates a repulsive potential that serves as an additional barrier for
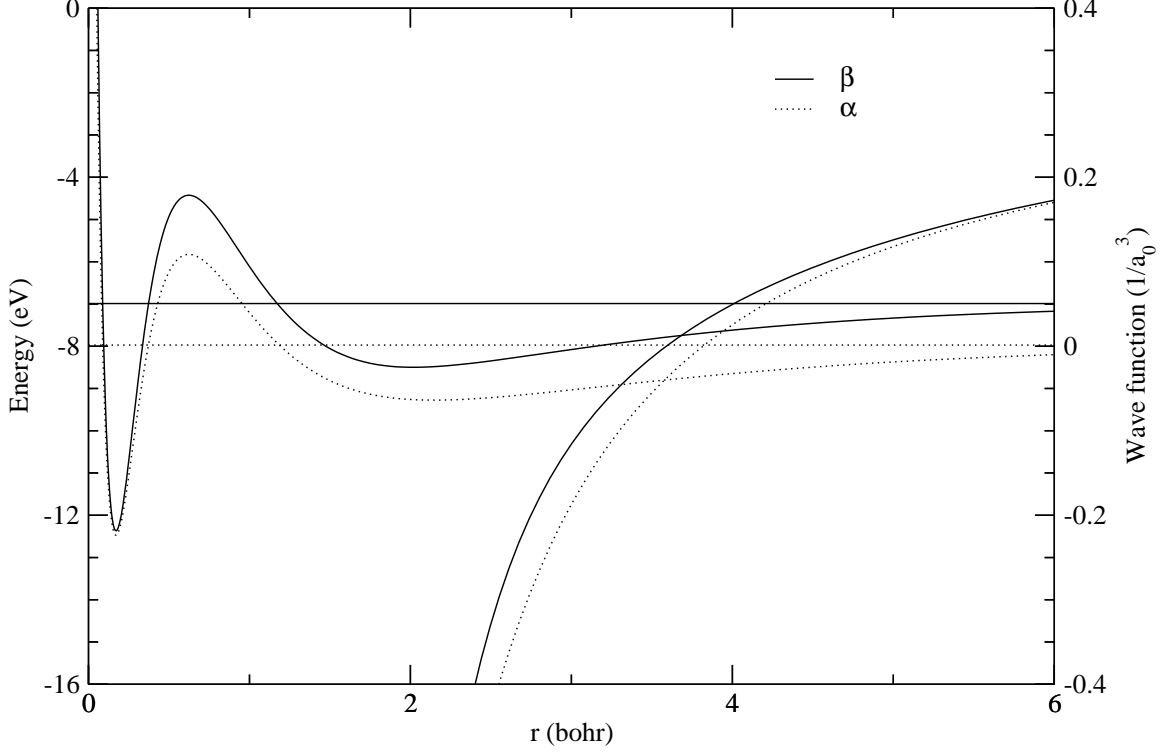
12

Figure 5: The α and β spin static KS potentials $v_\sigma(r, 0)$, the highest $(4s_\downarrow)$ and second highest $(4s_\uparrow)$ occupied orbital spin orbitals of the $^4F_{9/2}$ state and their energies. The wave functions are shifted vertically such that their zeros occur at the intersections with the corresponding energy levels.

tunneling ionization. As such, dynamics of the second electron creates a $\Delta v_\beta^{(0)}$ that binds the electron more to the core and a $\Delta v_\beta^{(1)}$ that increases the tunneling barrier.

For the $^6D_{9/2}$ sextet state, the two highest spin orbitals are plotted in Fig. 6. They both have α spin. The second highest electron occupies a $3d_\uparrow$ orbital and the combination of a lower energy level and an additional centrifugal barrier prevents the electron from tunneling out first. In contrast with the quartet case, both the Coulomb and the exchange terms contribute to the change in the KS potential

$$\Delta v_\alpha(\boldsymbol{r}, t) \approx \iiint \frac{\Delta\rho_{3d}(\boldsymbol{r}', t)}{|\boldsymbol{r} - \boldsymbol{r}'|} d^3\boldsymbol{r}' + \Delta V_{\text{xc},3d}(\boldsymbol{r}, t) + \Delta V_{\text{xc},3d4s}(\boldsymbol{r}, t). \tag{20}$$

Here, $\Delta\rho_{3d}$ is the change of density due to the dynamics of the $3d$ electrons, $\Delta V_{\text{xc},3d}$ is the change in the exchange potential caused by the $3d$ electrons only, and $\Delta V_{\text{xc},3d4s}$ is the change in the exchange between $3d$ and $4s$ electrons [see Eq. (12)]. At $r = 0.45\ a_0$, $3d$ electrons dominate the density and the first two terms of Eq. (20) mostly cancel each other. Away from this distance, $\Delta V_{\text{xc},3d}$ becomes insignificant. We therefore combine the first two terms
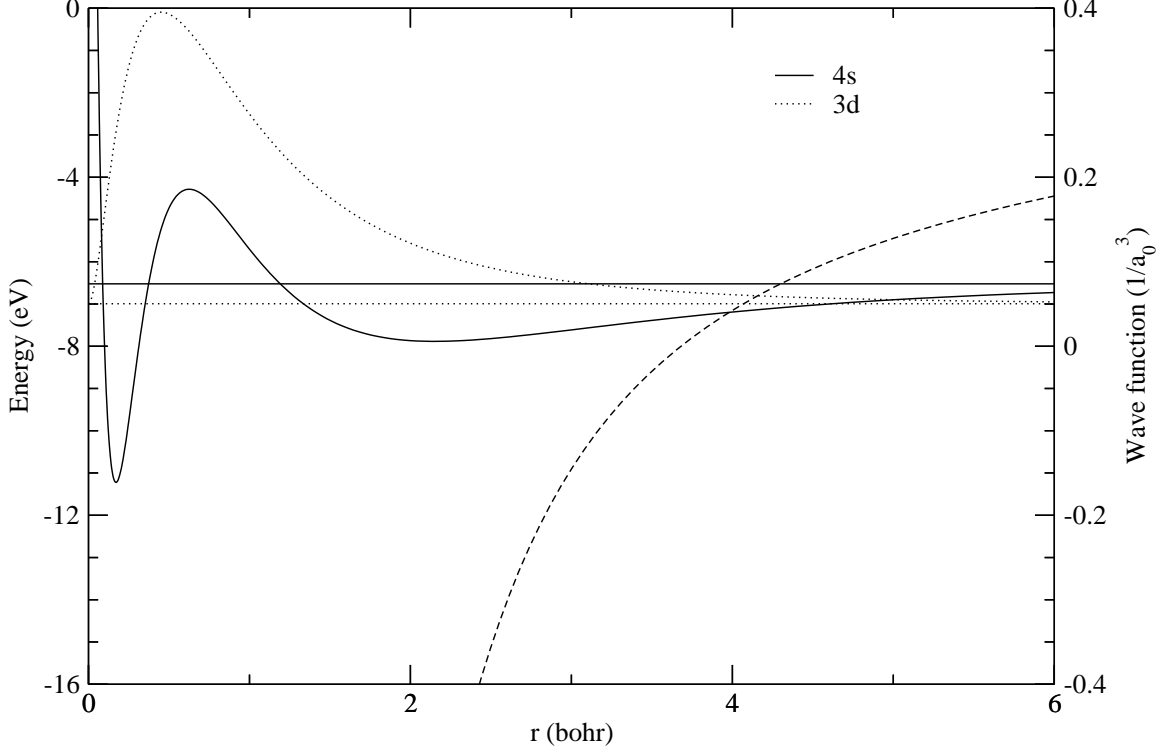
Figure 6: The α-electron Kohn-Sham potential for the ${}^6D_{9/2}$ state (dashed line), the highest $(4s_\uparrow)$ (solid line) and second highest $(3d_\uparrow)$ (dotted line) occupied orbitals and their energy levels. The wave functions are shifted vertically such that their zeros occur at the intersections with the corresponding energy levels.

and rewrite Eq. (20) as

$$\Delta v_\alpha(\boldsymbol{r}, t) \approx \iiint \frac{\Delta \tilde{\rho}_{3d}(\boldsymbol{r}', t)}{|\boldsymbol{r} - \boldsymbol{r}'|} d^3 \boldsymbol{r}' + \Delta V_{\text{xc},3d4s}(\boldsymbol{r}, t), \tag{21}$$

where $\Delta \tilde{\rho}_{3d}$ is an "effective change" of the density of $3d$ electrons, which takes into account cancellation due to the exchange term by reducing the density.

The first term of Eq. (21) expands similarly as in Eq. (18). The second term, however, causes $\Delta v_\alpha(\boldsymbol{r}, t)$ of the sextet to be very different from $\Delta v_\beta(\boldsymbol{r}, t)$ of the quartet. To understand this difference, we consider the first two terms in the Legendre expansion of the exchange contribution to the KS potential for the α electrons (see Section III A),

$$\begin{aligned} \Delta V_{xc,\alpha}^{3d4s}(r, t) \approx{} & -\frac{\rho_{4s,3d}^{(0)}(r, t) \int_0^r \rho_{3d,4s}^{(0)}(r', t) dr'}{r \rho_\alpha(\boldsymbol{r}, t)} - \frac{\rho_{4s,3d}^{(0)}(r, t)}{\rho_\alpha(\boldsymbol{r}, t)} \int_r^\infty \frac{\rho_{3d,4s}^{(0)}(r', t)}{r'} dr' \\ & - \left[\frac{\int_0^r \rho_{3d,4s}^{(1)}(r', t) r' dr'}{r^2 \rho_\alpha(\boldsymbol{r}, t)} + \frac{r \rho_{4s,3d}^{(1)}(r, t)}{\rho_\alpha(\boldsymbol{r}, t)} \int_r^\infty \frac{\rho_{3d,4s}^{(1)}(r', t)}{r'^2} dr \right] \cos(\theta) \\ & -c.c., \end{aligned} \tag{22}$$
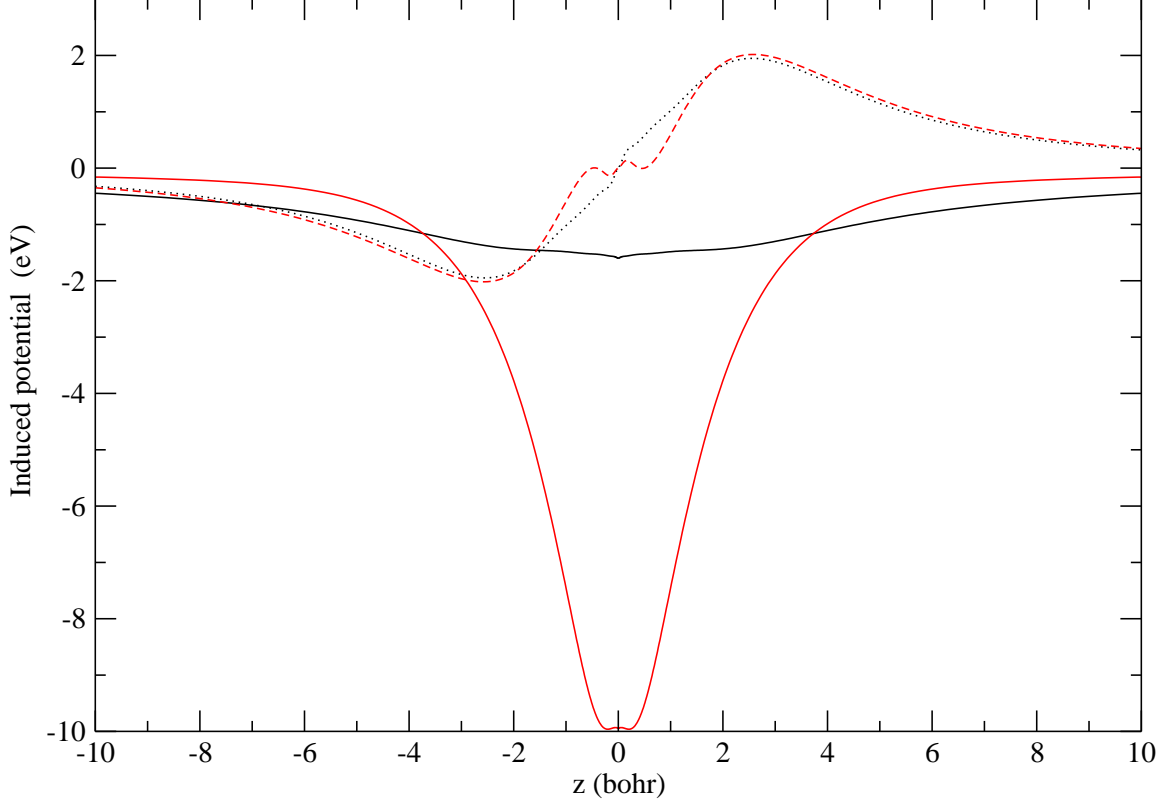
14

Figure 7: Induced potential, $\Delta v_\beta^{(l)}(r, t_m) P_l(\cos\theta)$ for $l = 0$ (solid) and $l = 1$ (dotted) of the ${}^4F_{9/2}$ quartet state (black) and $\Delta v_\alpha^{(l)}(r, t_m) P_l(\cos\theta)$ for $l = 0$ (solid), and for $l = 1$ (dashed) of the ${}^6D_{9/2}$ sextet state (red), at the peak intensity of a 1.54×10^{13} W/cm^2, 1500 nm laser. $t_m = T/2 + 3\pi/2\omega$.

where $\rho_{4s,3d}^{(l)}(r, t) = [\rho_{3d,4s}^{(l)}(r, t)]^*$. For unperturbed orbitals, $\rho_{3d,4s}^{(l)}(r, 0)$ is only nonzero for $l = 2$, so at $t = 0$ the two terms with $l = 0$ and $l = 1$ are zero. If we write both $\psi_{4s\uparrow}(\boldsymbol{r}, t)$ and $\psi_{3d\uparrow}(\boldsymbol{r}, t)$ orbitals as linear combinations of field free spin orbitals, we find that a nonzero $l = 0$ contribution only arises when both orbitals mix in atomic orbitals of the same angular momenta. For instance, both orbitals may mix in a $4p_z$ orbital. A nonzero $l = 1$ term arises from spin orbitals whose angular momentum quantum numbers differ by one.

In Fig. 7 we compare the induced KS potentials $\Delta v_\beta^{(0)}$ of the quartet with $\Delta v_\alpha^{(0)}$ of the sextet and $\Delta v_\beta^{(1)}$ of the quartet with $\Delta v_\alpha^{(1)}$ of the sextet at the maximum field strength of $I = 1.54 \times 10^{13}$ W/cm^2 at $t_m = T/2 + 3\pi/2\omega$. This peak intensity is chosen because the TDDFT calculated ionization probability of the quartet agrees well with the experimental data. We also consider that at this laser intensity, the atom is not too far away from the ground state to be treated with a local adiabatic exchange-correlation potential.
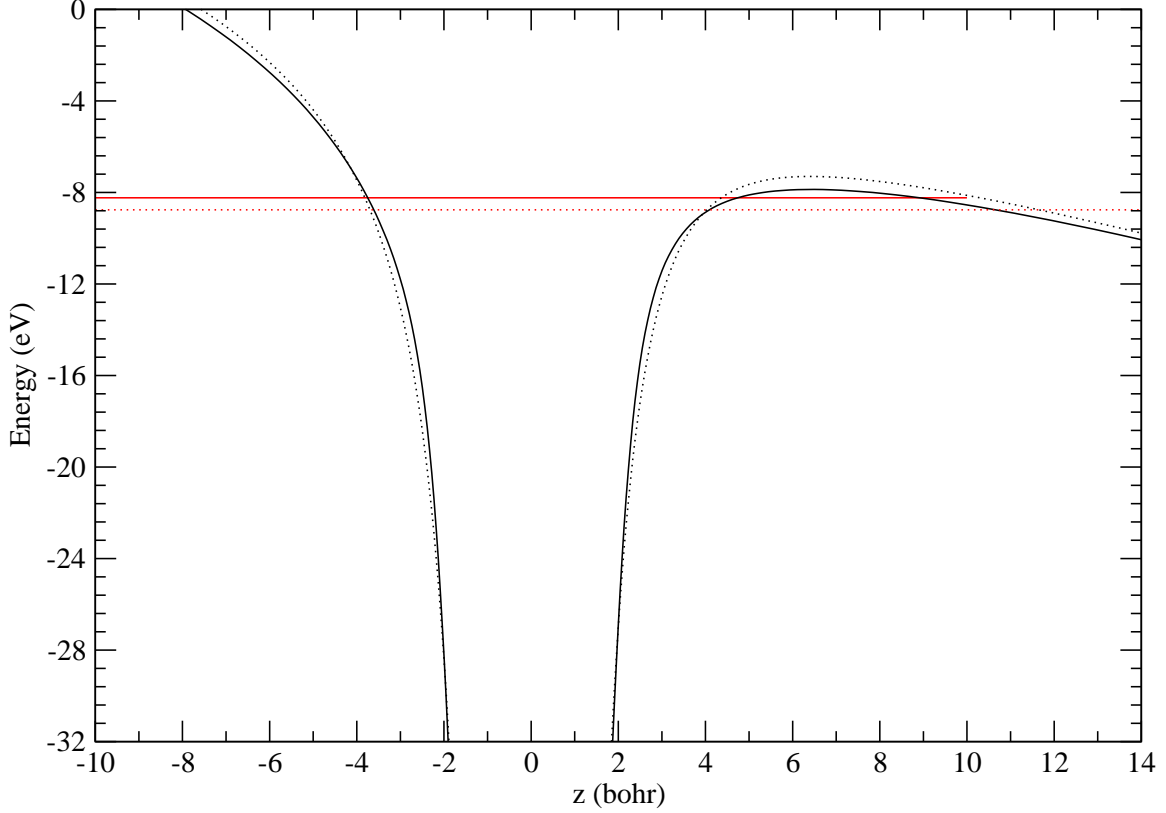
Figure 8: Energy diagram for vanadium in a 1500 nm laser of 1.54×10^{13} W/cm^2. Solid black line: the electronic potential at the peak intensity according to our TDDFT formalism for the quartet $^4F_{9/2}$. Dotted black line: the same potential for the sextet $^6D_{9/2}$. Solid red line: the shifted energy level for the quartet $^4F_{9/2}$. Dotted red line: the shifted energy level for the quartet $^4F_{9/2}$.

The induced isotropic potential $\Delta v_\alpha^{(0)}$ of the sextet is much more attractive than $\Delta v_\beta^{(0)}$ of the quartet at short radial distances. At the core, the ratio of these potentials is six. The two curves cross at $r = 3.7\ a_0$. Beyond this point, $\Delta v_\beta^{(0)}$ of the quartet is more attractive. The substantial difference near the core is caused by the first two terms of Eq. (22): in the strong laser field, the $3d$ and $4s$ mix in orbitals with the same angular momentum. For the sextet the electrons in these orbitals have the same spin, and exchange interaction lowers the time-dependent KS potential, increasing the ionization potential. For the quartet, the electrons in these orbitals have opposite spin, and there is no exchange interaction. Both $\Delta v_\alpha^{(1)}$ of the sextet and $\Delta v_\beta^{(1)}$ of the quartet peak at $r = 2.6\ a_0$ where they are about 2 eV. This elevates the ionization barrier and reduces the tunneling ionization rate for both states.

The effects of the induced KS potentials depicted in Fig. 7 on the full time-dependent KS potentials [Eq. (7)], including the electric field and the higher order Legendre terms,

16

are shown in Fig. 8. In black solid and dotted lines, we plot $v_\beta(\boldsymbol{r}, t_m)$ of the quartet and $v_\alpha(\boldsymbol{r}, t_m)$ of the sextet. At shorter radial distances ($r < 2.3\ a_0$) the two potentials become indistinguishable, contrary to corresponding static KS potentials in Fig. 3. This is due to the much lower $\Delta v_\alpha^{(0)}$ of the sextet shown in Fig. 7. To demonstrate the binding effect of this lowered potential of the sextet, we add the isotropic induced potentials (solid lines in Fig. 7) to the field free electronic potentials (black lines in Fig. 3) and calculate the shifted highest occupied energy levels of the quartet (red solid line in Fig. 8) and sextet (red dotted line in Fig. 8). The shifted energy level of the sextet becomes lower than that of the quartet by 0.53 eV.

Figure 8 also shows that the barrier for tunneling ionization is higher for the sextet than for the quartet. The peaks of the barriers are at $6.3\ a_0$ and the difference in the barrier heights is about 0.51 eV. Figure 7 shows that the difference in $\Delta v_\sigma^{(0)}$ accounts for most of it. The barrier width is larger for the sextet, which is due to the combination of a higher potential for $r > 4\ a_0$ and lower energy level.

VI. DISCUSSION AND CONCLUSIONS

Using a TDDFT method that incorporates the weighted Hartree Fock exchange into a time-dependent KS potential, we compare tunneling ionization of the $^4F_{9/2}$ and $^6D_{9/2}$ fine structure states of vanadium in intense lasers. For such a comparison we must discuss the deviation of $\langle S^2 \rangle$ from the exact value. In principle, the deviation is zero for the sextet but nonzero for the quartet since our method is spin unrestricted. The deviation is supposed to be smaller for a DFT method than for Hartree Fock method, but harder to estimate. For simplicity, we follow the formula for UHF,

$$\langle S^2 \rangle - \langle S^2 \rangle_{\text{exact}} = N_\beta - \sum_{i=1}^{N_\alpha} \sum_{j=1}^{N_\beta} |\langle \psi_{i\alpha} | \psi_{j\beta} \rangle|^2. \tag{23}$$

For $t = 0$ it is calculated to be 0.0003. Ionization occurs at $t > 0$ and the formula is not valid any more.

This deviation means that the calculated $4s_\downarrow$ spin orbital of the quartet is slightly contaminated with higher orbitals, which may lead to an insignificantly overestimated ionization yield. Without inclusion of the induced potential, the quartet renders higher ionization yield in spite of the contamination. The induced potential that substantially suppresses the

17

tunneling ionization in the sextet comes from dynamic exchange between $4s_\uparrow$ and $3d_\uparrow$, which does not affect the single electron ionization yield of the quartet. Therefore spin contamination does not hinder us from reaching the conclusion that the tunneling ionization rate of ^6D is lower than that of ^4F for vanadium, in spite of a lower ionization potential. Exchange blockade is the reason for the much lower ionization rate of the high spin state. It comes from the dynamic effect that the highest and second highest electron mix in the same spin orbitals in intense laser fields.

The ground state of niobium is $^6D_{1/2}$ and its ionization rates are much lower than the quartet ground state, $^4F_{3/2}$ of vanadium. Since niobium belongs to the same group as vanadium in the periodic table and the ground state electron configuration of niobium is $4d^45s$, we believe that the same exchange blockade as what we discover here for the sextet is the reason for the significant ionization suppression for niobium. We predict that the ionization rates for the quartet is much larger for niobium as well.

Acknowledgments

[1] R. Kienberger, M. Hentschel, M. Uiberacker, Ch. Spielmann, M. Kitzler, A. Scrinzi, M. Wieland, T. Westerwalbesloh, U. Kleineberg, U. Heinzmann, et al., Science **297**, 1144 (2002).

[2] F. Krausz and M. Ivanov, Rev. Mod. Phys. **81**, 163 (2009).

[3] L. V. Keldysh, Sov. Phys. JETP **20**, 1307 (1965).

[4] M. V. Ammosov, N. B. Delone, and V. P. Kraǐnov, Sov. Phys. JETP **64**, 1191 (1986).

[5] R. Torres, N. Kajumba, J. G. Underwood, J. S. Robinson, S. Baker, J. W. G. Tisch, R. de Nalda, W. A. Bryan, R. Velotta, C. Altucci, et al., Phys. Rev. Lett. **98**, 203007 (2007).

[6] X. Chu and G. C. Groenenboom, Phys. Rev. A **93**, 013422 (2016).

[7] R. Torres, T. Siegel, L. Brugnera, I. Procino, J. G. Underwood, C. Altucci, R. Velotta, E. Springate, C. Froud, I. C. E. Turcu, et al., Opt. Express **18**, 3174 (2010).

[8] X. Chu and G. C. Groenenboom, Phys. Rev. A **87**, 013434 (2013).

[9] M. Lezius, V. Blanchet, M. Y. Ivanov, and A. Stolow, J. Chem. Phys. **117**, 1575 (2002).

[10] M. Smits, C. A. de Lange, A. Stolow, and D. M. Rayner, Phys. Rev. Lett. **93**, 213003 (2004).

[11] T. Brabec, M. Côté, P. Boulanger, and L. Ramunno, Phys. Rev. Lett. **95**, 073001 (2005).

[12] Z. X. Zhao and T. Brabec, J. Phys. B **39**, L345 (2006).

[13] Z. Zhao and T. Brabec, J. Mod. Opt. **54**, 981 (2007).

[14] X. Chu and G. C. Groenenboom, Phys. Rev. A **94**, 053417 (2016).

[15] X.-M. Tong and S.-I. Chu, Phys. Rev. A **57**, 452 (1998).

[16] A. Zangwill and P. Soven, Phys. Rev. A **21**, 1561 (1980).

[17] E. Runge and E. K. U. Gross, Phys. Rev. Lett. **52**, 997 (1984).

[18] E. K. U. Gross and W. Kohn, Adv. Quant. Chem. **21**, 255 (1990).

[19] X. Chu and S.-I. Chu, Phys. Rev. A **64**, 063404 (2001).

[20] A. Kramida, Y. Ralchenko, J. Reader, and N. A. Team, *Nist atomic spectra database (version 5.3)*, online (2015), national Institute of Standards and Technology, Gaithersburg, MD., URL `http://physics.nist.gov/asd`.